Eur. Phys. J. A **19**, 347–354 (2004)
DOI 10.1140/epja/i2002-10310-7

THE EUROPEAN PHYSICAL JOURNAL A

Studies of multi-nucleon transfer reactions in ^{90}Zr(^{18}O, X) and ^{90}Zr(^{16}O, X)

V. Jha[1,a], B.J. Roy[1,2,b], A. Chatterjee[1], and H. Machner[2]

[1] Nuclear Physics Division, B.A.R.C., Mumbai - 400 085, India
[2] Institute of Kernphysik, Forschungszentrum, Juelich, Germany

Received: 12 September 2002 / Revised version: 24 September 2003 /
Published online: 27 January 2004 –
Communicated by D. Guerreau

Abstract. Multi-nucleon transfer reactions in ^{18}O + ^{90}Zr and ^{16}O + ^{90}Zr have been studied at an incident energy of 90 MeV. The energy spectra and angular distributions are measured. The data have been analyzed to obtain cross-section dependence on the number of nucleons transferred and on the ground-state Q-values. In the ^{90}Zr(^{18}O, X); X = ^{16}O, ^{17,16,15,14}N, ^{14,13,12}C, ^{12,11,10}B, ^{10,9,7}Be and ^{7,6}Li reactions, 2n and 2n-correlated transfer cross-sections are observed to be enhanced as compared to the ^{16}O + ^{90}Zr reaction. A detailed comparison in the multi-particle stripping and elastic-scattering cross-section between these two systems are made in order to investigate the possible influence of the two valence neutrons in ^{18}O nucleus. Diffractional model DWBA calculations, based on the direct surface transfer model, have been performed to understand the reaction mechanism of multi-nucleon transfer to continuum.

PACS. 25.70.Hi Transfer reactions – 25.70.Bc Elastic and quasielastic scattering

1 Introduction

Multi-nucleon transfer in heavy-ion reactions at energies above the Coulomb barrier can proceed through different reaction mechanisms with a continuous evolution from quasi-elastic transfer to deep inelastic regime. It is well known that the quasi-elastic transfer processes manifest themselves as bell-shaped angular distributions peaked near the grazing angle, whereas the processes involving massive transfer occur at relatively smaller internuclear distance and are generally more forward-peaked [1]. A recent review article [2] gives a good account of the multi-nucleon transfer between heavy nuclei. An important aspect of heavy-ion transfer reactions is the matching of various kinematical quantities, *e.g.* energy, angular momentum, etc., in the entrance and exit channels. Apart from the kinematical factors, projectile and target structure influence multi-nucleon transfer cross-section significantly. Recent observations of large enhancement in the 2n and 2n-correlated transfer cross-sections in ^{18}O + ^{174}Yb have been explained by interpreting the projectile as a core plus two loosely bound valence neutrons in a "di-neutron" configuration outside the relatively tightly bound ^{16}O core [3]. Such an interpretation for the nucleus ^{18}O, having a large two-neutron separation energy (12.19 MeV), certainly needs further investigations. With a motivation to study the possible role of two valence neutrons in the ^{18}O nucleus on multiparticle stripping cross-section we have studied, in the present work, multi-nucleon transfer reactions in the two systems ^{18}O + ^{90}Zr and ^{16}O + ^{90}Zr measured under same kinematical conditions. A detailed comparison between these two systems in the multi-nucleon transfer channels as well as elastic-scattering process has been made to shed more light on these aspects. The energy spectrum and angular distribution for multi-nucleon transfer reactions to continuum are analyzed in the DWBA-based diffractional model (DDWBA) calculations [4]. Such DDWBA calculations, based on direct surface transfer reaction model, have been used in the past [5–8] and are quite successful for the description of multi-nucleon transfer processes to the continuum. The results of the analysis are presented and discussed here.

2 Experimental procedure

The measurements were carried out using ^{16}O and ^{18}O beams of 90 MeV incident energy from the 14UD Pelletron accelerator in Mumbai. Isotopically enriched ($\geq$ 99%) self-supporting ^{90}Zr targets of 400 μg/cm^2 thickness were used. Light ejectiles were detected using silicon surface barrier detector telescopes (ΔE = 30 μm and

[a] e-mail: vjha@magnum.barc.ernet.in
[b] e-mail: b.roy@fz-juelich.de

Table 1. Measured differential cross-sections for various reaction channels in ^{16}O + ^{90}Zr and ^{18}O + ^{90}Zr both studied at the same incident energy of 90 MeV and $\theta_{\rm lab} = 20^\circ$. The differential cross-sections listed here are for the excitation energy integrated data. The reaction Q-values (Q_0) listed in the table are ground-state Q-values.

Reaction	Q_0 (MeV)	dσ/dΩ (mb/sr)	Reaction	Q_0 (MeV)	dσ/dΩ (mb/sr)
			^{90}Zr(^{18}O,^{16}O)	+3.642	34.90 ± 0.35
			^{90}Zr(^{18}O,^{17}N)	−10.783	1.95 ± 0.08
			^{90}Zr(^{18}O,^{16}N)	−8.783	1.64 ± 0.08
^{90}Zr(^{16}O,^{15}N)	−6.948	15.76 ± 0.32	^{90}Zr(^{18}O,^{15}N)	−2.443	12.56 ± 0.21
^{90}Zr(^{16}O,^{14}N)	−9.915	7.55 ± 0.22	^{90}Zr(^{18}O,^{14}N)	−6.047	2.34 ± 0.09
^{90}Zr(^{16}O,^{13}N)	−11.642	1.33 ± 0.09	^{90}Zr(^{18}O,^{13}N)		
^{90}Zr(^{16}O,^{14}C)	−9.718	5.82 ± 0.20	^{90}Zr(^{18}O,^{14}C)	−4.159	9.71 ± 0.18
^{90}Zr(^{16}O,^{13}C)	−9.827	13.87 ± 0.30	^{90}Zr(^{18}O,^{13}C)	−4.968	7.47 ± 0.16
^{90}Zr(^{16}O,^{12}C)	−5.094	37.83 ± 0.51	^{90}Zr(^{18}O,^{12}C)	−0.760	10.57 ± 0.19
^{90}Zr(^{16}O,^{12}B)	−22.718	0.25 ± 0.04	^{90}Zr(^{18}O,^{12}B)	−17.102	0.11 ± 0.02
^{90}Zr(^{16}O,^{11}B)	−16.157	2.65 ± 0.13	^{90}Zr(^{18}O,^{11}B)	−10.998	1.20 ± 0.06
^{90}Zr(^{16}O,^{10}B)	−19.734	0.68 ± 0.07	^{90}Zr(^{18}O,^{10}B)	−15.173	0.21 ± 0.03
^{90}Zr(^{16}O,^{10}Be)	−19.484	0.14 ± 0.03	^{90}Zr(^{18}O,^{10}Be)	−13.934	0.11 ± 0.02
^{90}Zr(^{16}O,^{9}Be)	−18.741	0.47 ± 0.06	^{90}Zr(^{18}O,^{9}Be)	−13.282	0.44 ± 0.04
^{90}Zr(^{16}O,^{7}Be)	−21.658	0.09 ± 0.03	^{90}Zr(^{18}O,^{7}Be)	−17.370	0.03 ± 0.01
^{90}Zr(^{16}O,^{7}Li)	−22.865	0.23 ± 0.04	^{90}Zr(^{18}O,^{7}Li)	−17.049	0.21 ± 0.03
^{90}Zr(^{16}O,^{6}Li)	−22.002	0.22 ± 0.04	^{90}Zr(^{18}O,^{6}Li)	−16.825	0.16 ± 0.03

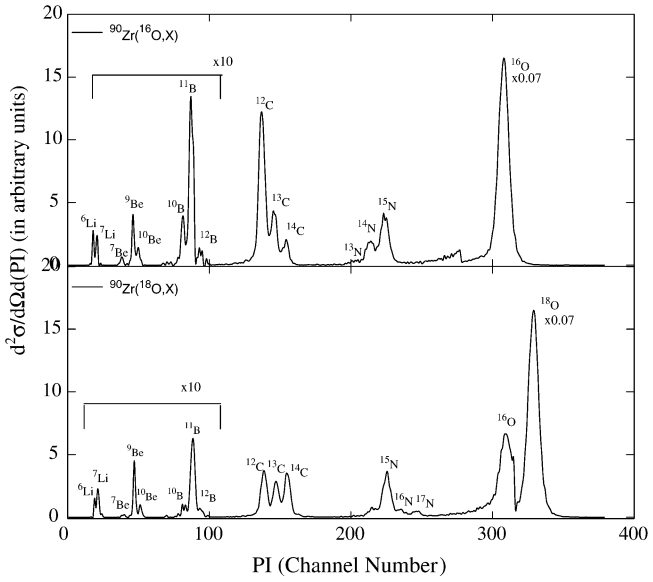

Fig. 1. Counts *vs.* particle identification (PI) spectra generated from a two-dimensional PI *vs.* energy plot by taking the projection on the PI axis.

$E = 300$ μm) mounted on two movable arms inside a 1 m diameter scattering chamber. The detailed experimental procedure is the same as described previously [9] and hence is not repeated here. Particle identification (PI) spectra for both systems are shown in fig. 1. It has been possible, using the $\Delta E - E$ technique, to obtain not only charge but also a good mass separation between various projectile-like particles thus allowing us to make a detailed study of multi-nucleon transfer reactions in these two systems. The Q-integrated cross-sections for various reaction channels are listed in table 1. Though the values for the ^{16}O + ^{90}Zr have already been reported in our previous publication [9], they have been given here for comparison purposes. The errors given in the table are the statistical ones. In addition, an overall systematic uncertainty of 13% is estimated. The measured laboratory angular distribution for the dominant transfer channels in both the systems is shown in fig. 2.

3 Results and discussion

The total cross-sections, obtained by integrating the differential distributions, are plotted as a function of the number of nucleons transferred x in fig. 3. In general, the cross-section decreases as the number of transferred nucleons increases. In the ^{16}O + ^{90}Zr system, the projectile-like products strongly populated are ^{15}N, ^{14}N, ^{14}C, ^{13}C, ^{12}C, ^{11}B, ^{10}B, ^{9}Be, ^{7}Li, ^{6}Li, etc., corresponding to a transfer of 1p, (1p1n), 2p, (2p1n), α, (αp), (αpn), (α2p1n), etc., with 1p and α transfer reactions being the strongest. Interestingly, ^{18}O + ^{90}Zr reactions also populate same projectile-like products now corresponding to a transfer of (1p+2n), (1p1n+2n), (2p+2n), (2p1n+2n), (α+2n), (αp+2n), (αpn+2n), (α2p1n+2n), etc., nucleons, respectively. The 2n transfer reaction (the only positive Q-value reaction) has largest cross-section and (α+2n) transfer is stronger than α transfer. Also observed is the single-nucleon transfer, usually the most dominant reaction channel, a factor of 6 lower in cross-section as compared to the 1p+2n transfer. Usually, the transfer cross-section decreases exponentially with the increasing number of nucleons transferred. The present observation suggests a possible influence of the projectile structure on multi-nucleon stripping reactions.

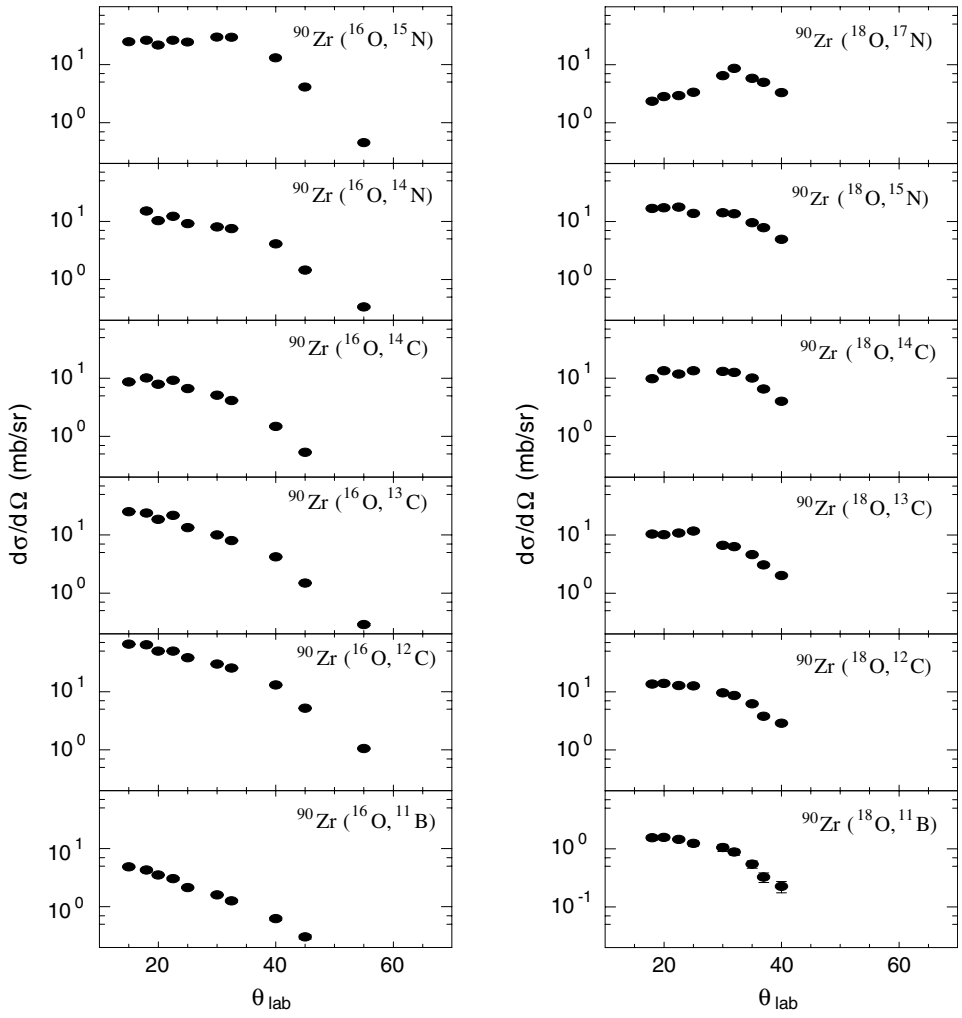

Fig. 2. Measured laboratory angular distribution of dominant transfer channels in ^{16}O + ^{90}Zr and ^{18}O + ^{90}Zr at $E_{\rm lab} = 90$ MeV.

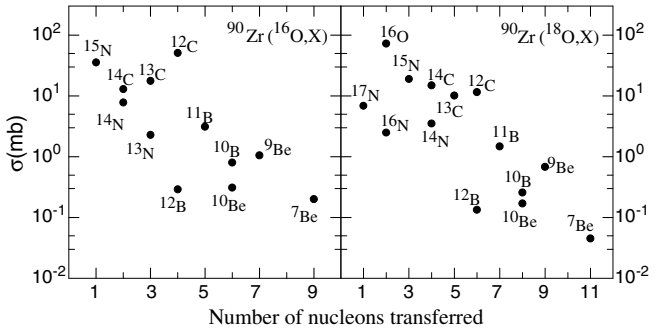

Fig. 3. Total cross-section plotted as a function of the number of nucleons transferred in ^{16}O + ^{90}Zr and ^{18}O + ^{90}Zr reactions.

To understand this, the Q-value dependence of the cross-section has been studied. From earlier studies [10–19], it is known that the differential cross-section for isotope production of each charge decreases exponentially with increasing negativity of ground-state Q-value (Q_0) ($\mathrm{d}\sigma/\mathrm{d}\Omega \sim e^{Q_0/T}$) and is understood in the picture of a partially statistical equilibrium of a di-nuclear system with an effective temperature T. The same exponential dependence can also be explained in the framework of direct reaction mechanism where the slope parameter T is related to the mean energy loss per transferred nucleon and the probability for single-nucleon transfer [15]. The measured cross-sections for the production of N, C, B and Be isotopes are plotted in fig. 4. Yields for different isotopes of a given element follow, in general, the exponential dependence and slopes for different elements are about the same, with some exception in the case of beryllium isotopes where a much steeper slope has been observed in both the ^{16}O- and ^{18}O-induced reactions. Similar irregularities in the Q_0 systematics have also been observed in previous studies [13,14] and have been systematized by taking effects of pairing energies into account. The importance of such pairing energy corrections (Δ) (so-called "non-pairing" corrections) has been emphasized in those works and is observed to have a significant effect in reactions with Zr target and less pronounced with other systems. The present data (the Q_0-values) have been corrected for the pairing energies and are re-plotted in fig. 5 (in a bit different way for the comparison purposes between

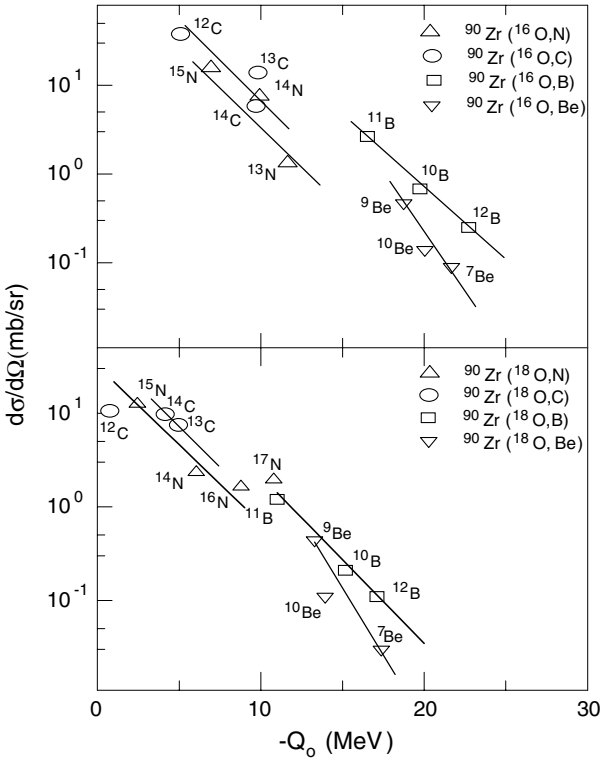

Fig. 4. Differential cross-section for the projectile-like products of the ^{90}Zr(^{16}O, X) and ^{90}Zr(^{18}O, X) reactions at $\theta_{\rm lab} = 20^\circ$ and $E_{\rm lab} = 90$ MeV plotted as a function of ground-state Q-value (Q_0). The lines are merely to guide the eye.

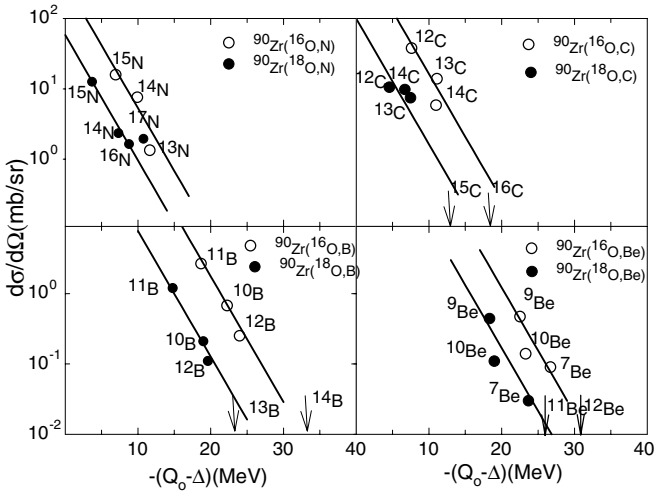

Fig. 5. Isotope production cross-section as a function of ground-state Q-value. Similar to fig. 4 but with non-pairing corrections (Δ) added and plotted in a bit different way for the comparison purposes between the ^{90}Zr(^{16}O, X) and ^{90}Zr(^{18}O, X) reactions. The arrows shown in the figure indicate the position of Q_0 for ^{90}Zr(^{18}O, X).

the two systems studied). A significant improvement has been obtained. The data for all elements now follow a single slope corresponding to an effective temperature of $T \sim 2.45$ MeV and is independent of projectile combination. It is to mention that the present value of the parameter T is similar to those obtained from other reactions [14].

The reason behind the absence of/the very low cross-section of 1p, 1p1n, 2p, 2p1n, α, αp, etc., transfer in the ^{18}O-induced reactions, which are quite strongly populated in the ^{16}O + ^{90}Zr reactions, can be simply explained in terms of this Q-value systematics. The Q-values for the 2n and 2n-correlated transfer channels are less negative in ^{18}O + ^{90}Zr and hence the cross-sections for these channels are enhanced. For example, the 2p transfer (^{90}Zr(^{18}O,^{16}C)) and 2p1n transfer (^{90}Zr(^{18}O,^{15}C)) reactions which are seen with large cross-section in the ^{16}O-induced reactions, are not observed in the ^{18}O case. The reason, as is clear from fig. 5, is due to a large negative Q-value for these channels (the Q_0-values for these reactions are indicated by arrows in fig. 5) as compared to the (^{18}O,^{14}C) and (^{18}O,^{13}C) reactions. Similarly, in the case of nitrogen isotopes, the cross-section for the one-nucleon transfer (^{16}O,^{15}N) is the highest which is then followed by the two-nucleon and three-nucleon transfer reactions. In the (^{18}O, N) case, the cross-section for three-nucleon transfer is larger compared to the corresponding one- and/or two-nucleon transfer channels as the Q-value for this three-nucleon transfer reaction is relatively much less negative (fig. 5). The explanation can very well be extended to other isotopes and is clear from the figure. Hence it is clear that the observed large yields in the 2n and 2n-correlated transfer reactions seen in the ^{90}Zr(^{18}O, X) reactions are due to the Q-value effect and the data can be well accounted for by the Q-value systematics.

The dependence of optimum Q-value ($Q_{\rm opt}$) on the number of nucleons transferred x has been studied for these two systems. A number of earlier works exist in the literature on $Q_{\rm opt}$ studies in heavy-ion transfer reactions [16–18,20,21] and different models have been proposed [18,20,21] to calculate the optimum Q-value $Q_{\rm opt}$. We follow the prescription [18], as has also been used in our previous study [19], that gives a satisfactory description to both charge and mass dependence of the observed $Q_{\rm opt}$. The effective optimum Q-value due to the matching of relative velocities at the distance of closest approach, immediately before and after the transfer, is defined as

$$Q_{\rm opt}^{\rm eff} = Q_{\rm opt} + \Delta E_{\rm C} = \epsilon_f - \epsilon_i = -(x/\mu_i)\epsilon_i\,, \qquad (1)$$

where x is the net number of nucleons transferred and μ_i the reduced mass of the entrance channel. ϵ_i is the available energy at the barrier and $\Delta E_{\rm C}$ is defined as the difference between the exit and entrance channel Coulomb barrier. The inclusion of the effect of kinetic energy loss due to frictional force in addition to momentum transfer modifies the above expression as

$$Q_{\rm opt}^{\rm eff} = -\Big[1 - (1 - x/\mu_i)\exp[-\alpha x/\mu_i]\Big]\epsilon_i\,. \qquad (2)$$

α is related to the frictional constant which is fixed for all exit channels and depends only on the entrance channel. α was kept as a free parameter. The calculated $Q_{\rm opt}$ values along with experimental points are plotted in fig. 6. A good agreement with almost same value of frictional

Table 2. Optical-Model parameters.

Reaction	V_0 (MeV)	r_0 (fm)	a_0 (fm)	W_i (MeV)	r_i (fm)	a_i (fm)	r_c (fm)	$\sigma_{\rm R}$ mb
^{90}Zr(^{12}C,^{12}C)	100.0	0.982	0.782	80.00	0.982	0.782	1.25	
^{90}Zr(^{16}O,^{16}O)	135.7	1.154	0.509	29.93	1.207	0.457	1.25	1445
^{90}Zr(^{18}O,^{18}O)	135.7	1.167	0.509	29.93	1.207	0.457	1.25	1500

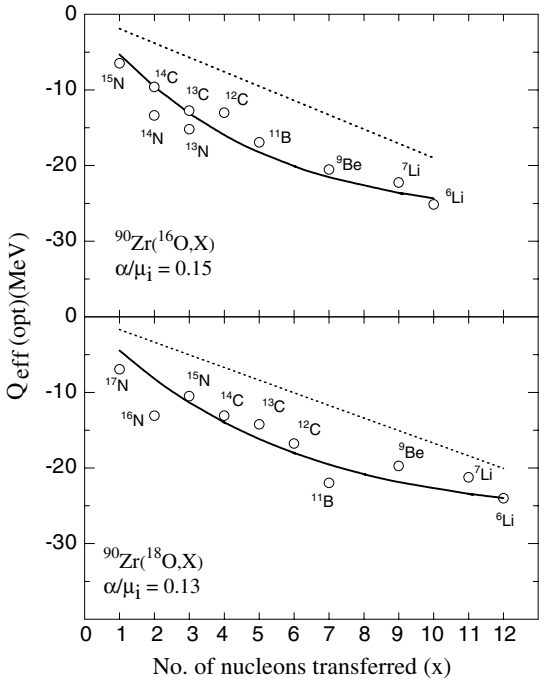

Fig. 6. Effective optimum Q-value as a function of the number of transferred nucleons x for the ^{90}Zr(^{16}O, X) and ^{90}Zr(^{18}O, X) reactions. The solid lines are the results of calculation as detailed in the text. The dotted lines correspond to a situation in the absence of frictional force and equivalent to the one described in ref. [14].

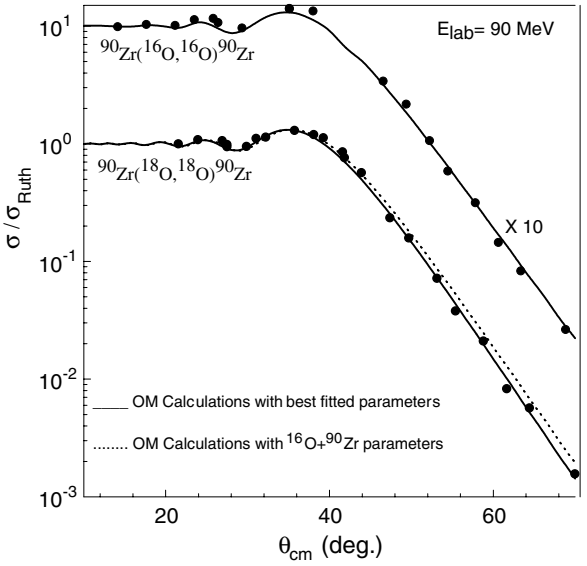

Fig. 7. Measured elastic-scattering angular distributions of ^{90}Zr(^{16}O,^{16}O)^{90}Zr and ^{90}Zr(^{18}O,^{18}O)^{90}Zr both measured at an incident energy of 90 MeV. The optical-model fits to the data (solid lines) are also shown. The dotted curve is the result with the best-fitted ^{16}O + ^{90}Zr parameters.

coefficient (α/μ) for both the systems has been obtained. For both the systems, the effective optimum Q-value approaches the same asymptotic value of ~ -25 MeV.

The measured elastic-scattering angular distribution of the two systems ^{18}O + ^{90}Zr and ^{16}O + ^{90}Zr has been compared and the possible influence of two valence neutrons in ^{18}O nucleus has been investigated. The data have been analyzed using the optical-model program SNOOPY [22]. A Woods-Saxon volume form of real and imaginary potentials was used. The OM potentials of ^{12}C + ^{90}Zr [23] are used as starting parameters for the analysis of ^{16}O + ^{90}Zr data. A search was made on all the parameters and the resulting parameters for which a best fit was obtained are given in table 2. These parameters are used as starting potentials for the analysis of the ^{18}O + ^{90}Zr elastic angular distribution. The same potential gives a good description of the ^{18}O + ^{90}Zr elastic scattering as well (shown by the dotted line in the fig. 7). Only a small variation of r_0 ($\sim$ 1% increase), the radius parameter for the real part of the potential, was needed to achieve the best fit to the data (solid line). The final parameters are given in the last column of table 2. The present study also observes a small ($\sim$ 4%) increase in the reaction cross-section in going from ^{16}O + ^{90}Zr to ^{18}O + ^{90}Zr. The almost equal values of the potential parameters (except only a small $\sim$ 1% increase in radius) suggest that the two valence neutrons in the ^{18}O nucleus have no significant influence on the elastic scattering and OM potential compared to the elastic scattering with the core ^{16}O nucleus.

4 Analysis of energy spectra and angular distributions in the diffractional DWBA model

The measured energy spectra and angular distributions of projectile-like particles have been analyzed in the DWBA-based diffractional model formalism. In this model the double differential cross-section to the continuum states

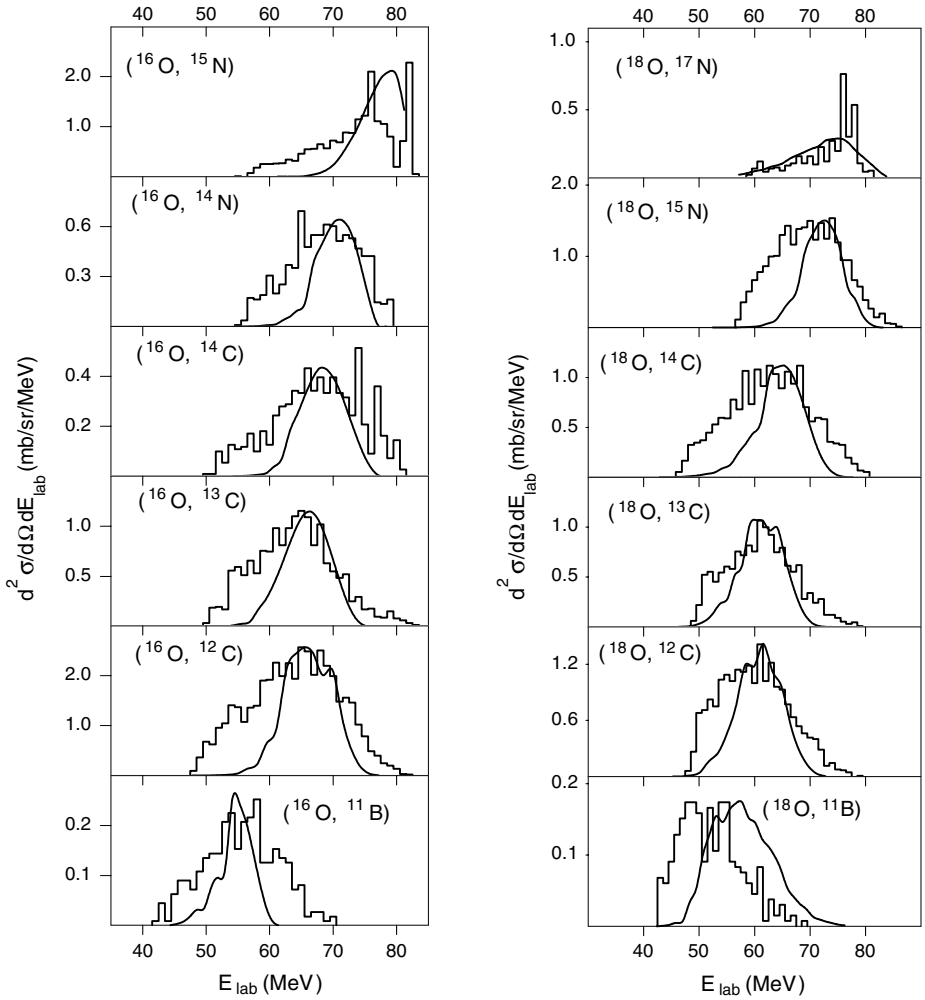

Fig. 8. Energy spectra of the projectile-like products observed in the ^{90}Zr(^{16}O, X) and ^{90}Zr(^{18}O, X) reactions at $\theta_{\rm lab} = 20^\circ$ and $E_{\rm lab} = 90$ MeV (shown as histograms). The solid lines show the energy spectra predicted by the calculations.

is given by [24,25]

$$\frac{\mathrm{d}^2\sigma}{\mathrm{d}\Omega \mathrm{d}E_f} = \sum_{J1,J2} \sum_{J1-J2}^{J1+J2} \int_0^{E_0^*} \rho_1(E_0^* - E_2^*, J2) \times \rho_2(E_2^*, J_2)\sigma(E_f, \theta, L_T)\mathrm{d}E_2^* \,. \quad (3)$$

The indices 1 and 2 are for the projectile-like particles and residual nucleus, respectively, and $\sigma(E_f, \theta, L_T)$ is the reduced transfer cross-section which is related to the DWBA transition matrix element as detailed in [24,25]. The spin-dependent form of the level density

$$\rho(E^*, J) = \rho(E^*)\frac{(2J+1)}{2\sqrt{2\pi}\sigma_{\rm cutoff}^3} e^{\frac{-J(J+1)}{2\sigma_{\rm cutoff}^2}} \quad (4)$$

is used. $\sigma_{\rm cutoff}$ is the spin cutoff parameter and $\rho(E)^*$ is the level density of particles and holes in the ejectile and residual nucleus. The level densities are calculated according to the Oblizinsky formula [26]. The reduced cross-section is parametrized in terms of three parameters: the radius parameter (r_0), the diffusivity (d) and the phase angle $\Delta\theta$, which is defined as the difference between the Coulomb and nuclear rainbows. This set of parameters have been deduced from the optical-model analysis of elastic-scattering data and are listed in table 3. The values are close to the recommended values of Mermaz *et al.* [27]. The results so obtained for the kinetic energy spectra and angular distributions are displayed in figs. 8 and 9. The calculated values were normalized to the experimental data as the spectroscopic information to the continuum states could not be supplied in the calculations.

Table 3. Kinematical quantities and diffractional model parameters deduced from the optical-model fits to the elastic scattering.

Reaction	r_0 (fm)	d (fm)	$\Delta\theta$ (rad)	$L_{\rm gr}$	$\theta_{\rm gr}$ (deg.)
^{90}Zr(^{16}O,^{16}O)^{90}Zr	1.5	0.28	0.41	46	48
^{90}Zr(^{18}O,^{18}O)^{90}Zr	1.51	0.26	0.41	47	49

The calculations predict the experimental energy spectra reasonably well. The peak is well reproduced whereas

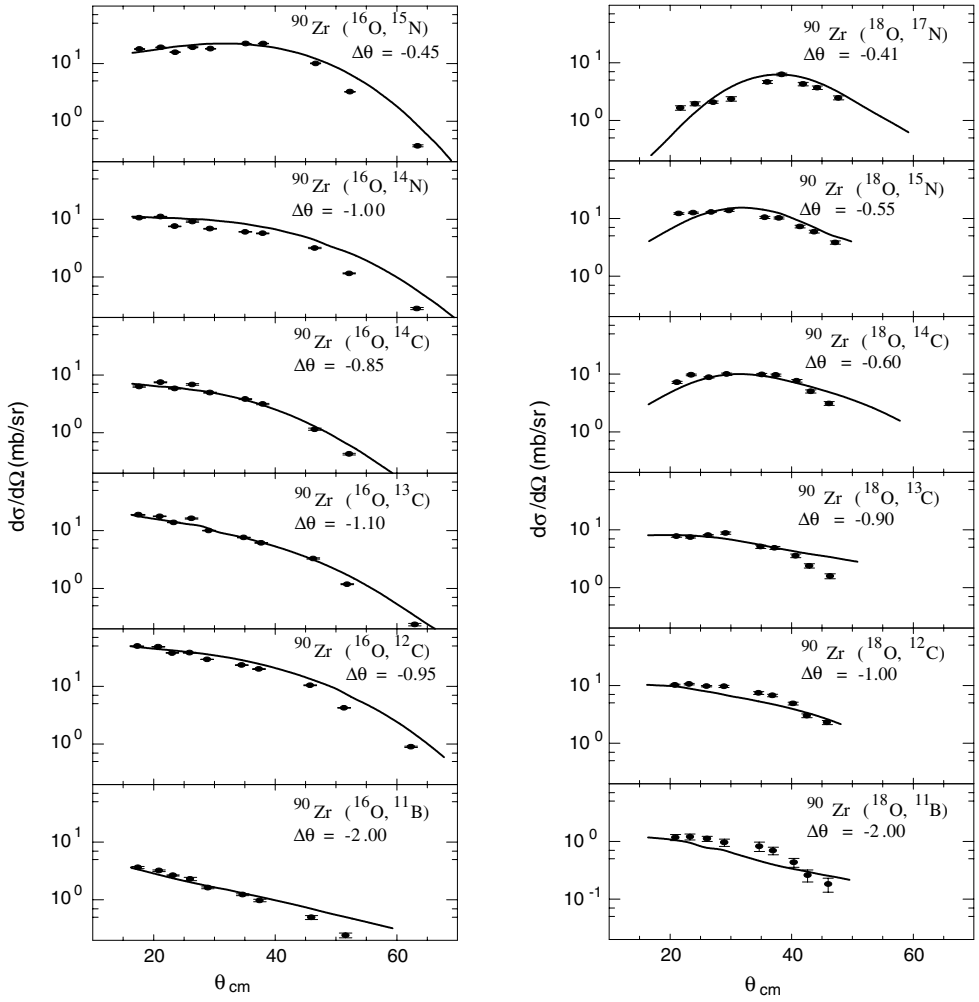

Fig. 9. Angular distributions of dominant transfer channels in the ^{16}O + ^{90}Zr and ^{18}O + ^{90}Zr. The solid lines are the diffractional model calculations. See the text for details.

the predicted shape of the kinetic energy spectra are in general narrower compared to the observed one. The lower energy part of the experimental spectra which corresponds to a higher excitation energy, in particular, is not described by the calculations. This is expected as this part of the spectrum can be attributed to more dissipative and multi-step processes and are not included in the present calculations which are based on direct surface transfer model. In fig. 9, the energy integrated angular distributions are compared with the model predictions. The observed angular distributions are bell-shaped for the one-nucleon transfer reactions peaked near $\sim 40^\circ$, about 10° lower than the grazing angle, and become more forward-peaked with the increasing number of nucleons transferred. The shape of the one-nucleon transfer reactions is reproduced well by the calculations. In order to reproduce the measured spectra for more-than-one-nucleon transfer, it was necessary to increase the values of $\Delta\theta$. The $\Delta\theta$ values used in the calculations are indicated in the figure. Such a practice of using larger values of $\Delta\theta$ than obtained from the elastic-scattering fit has been followed in the literature [25] to describe transfer angular distributions especially when the number of nucleons transferred is large. The necessity of larger values of $\Delta\theta$ with the increasing number on nucleons transferred is an indication of the increasing importance of nuclear effects and a continuous evolution from quasi-elastic transfer to the more dissipative processes.

5 Conclusions

The energy spectrum and differential cross-section of multi-nucleon transfer reactions in (^{16}O, X) and (^{18}O, X) with X = ^{16}O, ^{17,16,15,14}N, ^{14,13,12}C, ^{12,11,10}B, ^{10,9,7}Be and ^{7,6}Li, have been measured on the same target ^{90}Zr and at the same incident energy of 90 MeV. Transfer of up to 12 nucleons has been observed with significant cross-section. A clear charge and isotope separation for light ejectiles from lithium to oxygen has been achieved. The cross-sections for 2n and 2n-correlated transfer channels are seen to be enhanced in the ^{18}O + ^{90}Zr system. The data, when plotted as a function of ground-state Q-value for different isotopes, are understood in terms of Q-value

systematics. The charge and mass dependence of optimum Q-value are described in a model that takes into account the energy loss due to both momentum transfer and frictional force with only a single adjustable parameter α, the frictional constant. An almost equal value of the frictional coefficient (α/μ_i) has been obtained for both the systems and both the systems approach the same asymptotic value of effective optimum Q-value ~ -25 MeV.

The measured elastic-scattering angular distributions of these two systems are compared. The effect of two extra neutrons in ^{18}O is not significant on the elastic-scattering angular distribution and on the optical potential (only a small $\sim 1\%$ increase in the radius parameter) as compared to the $^{16}\mathrm{O} + {}^{90}\mathrm{Zr}$ case.

The energy spectra and angular distributions of projectile-like particles observed in these two systems are analyzed in the diffractional model DWBA formalism considering one-step peripheral process. The calculations reproduce the energy spectra reasonably well. The angular distributions are well described by increasing the difference between the Coulomb and nuclear phase angle as the number of nucleon transfer increases. A continuous evolution from the quasi-elastic to the more dissipative processes has been observed.

One of the authors (BJR) would like to thank Dr. M.G. Betigeri, Mr. B. Srinivasan and Mr. H.S. Patel for their help and interest during the early stages of this work. The excellent support of the operation staff of the Pelletron accelerator is greatly appreciated.

References

1. R. Bass, *Nuclear Reactions with Heavy Ions, Texts and Monographs in Physics*, Vol. **VIII** (Springer, Verlag, 1980).
2. W. von Oertzen, A. Vitturi, Rep. Prog. Phys. **64**, 1247 (2001) and references therein.
3. P.K. Sahu, R.K. Choudhury, D.C. Biswas, B.K. Nayak, Phys. Rev. C **64**, 014609 (2001).
4. N. Austern, J.S. Blair, Ann. Phys. (N.Y.) **33**, 15 (1965); F.J.W. Hahne, Nucl. Phys. A **104**, 545 (1967).
5. M.C. Mermaz, Phys. Rev. C **21**, 2356 (1980).
6. M.C. Mermaz , J. Barrette, H.E. Wegner, Phys. Rev. C **24**, 2148 (1981).
7. M.C. Mermaz, F. Auger, B. Fernandez, Phys. Rev. C **28**, 1587 (1983).
8. R.I. Badran, I.M. Naqib, D.J. Parker, J. Asher, J. Phys. G Nucl. Part. Phys. **22**, 1441 (1996).
9. V. Jha, B.J. Roy, A. Chatterjee, H.S. Patel, B. Srinivasan, M.G. Betigeri, H. Machner, Eur. Phys. J. A **15**, 389 (2002).
10. A.Y. Abul-Magd, K. El-Abed, M. El-Nadi, Phys. Lett. B **39**, 166 (1972).
11. A.G. Artukh, G.F. Gridnev, V.L. Mikkeev, V.V. Volkov, J. Wilczynski, Nucl. Phys. A **215**, 91 (1973).
12. V.V. Volkov, *Classical and Quantum Mechanical Aspects of Heavy-Ion Collisions*, edited by H.L. Harney, P. Braun-Munzinger, C.K. Gelbke (Springer-Verlag, Heidelberg, 1975) p. 253.
13. C.K. Gelbke, C. Olmer, M. Bienerd, D.L. Hendrie, J. Mahoney, M.C. Mermaz, D.K. Scott, Phys. Rep. **44**, 311 (1978).
14. V.V. Volkov, Phys. Rep. **44**, 93 (1978).
15. S.Y. Lee, P. Barun-Munzinger, Phys. Rev. C **24**, 1343 (1981).
16. T. Mikumo, T. Kohno, K. Katori, T. Motobayashi, S. Nakajima, M. Yoshie, H. Kamitsubo, Phys. Rev. C **14**, 1458 (1976).
17. J.S. Karp, S.G. Steadman, S.B. Gazes, R. Ledoux, F. Videbaek, Phys. Rev. C **25**, 1838 (1982).
18. Y. Alhassid, R.D. Levine, J.S. Karp, S.G. Steadman, Phys. Rev. C **20**, 1789 (1979).
19. B.J. Roy, B. Srinivasan, E. Shallom, M.G. Betigeri, H.C. Jain, M.L. Jhingan, Nucl. Phys. A **597**, 151 (1996).
20. P.J.A. Buttle, J.L.B. Goldfarb, Nucl. Phys. A **176**, 299 (1971).
21. P.J. Siemens, J.P. Bondorf, D.H.E. Gross, F. Dickmann, Phys. Lett. B **36**, 24 (1971).
22. P. Schwandt, optical model code SNOOPY8Q, Indiana University (1984).
23. S.T. Thoronton, D.E. Gustafson, J.L.C. Ford jr., K.S. Toth, D.C. Hensley, Phys. Rev. C **13**, 1502 (1976).
24. M.C. Mermaz, Phys. Rev. C **36**, 1000 (1987).
25. A. Pagano, S. Aiello, E. De Filippo, G. Lanzano, S. Lo. Nigro, C. Milone, G. Blancato, G. Di Marco, M.C. Mermaz, Phys. Rev. C **47**, 1170 (1993).
26. P. Oblozinsky, Nucl. Phys. A **453**, 330 (1986).
27. M.C. Mermaz, Phys. Lett. B **155**, 330 (1985).